Research in Astronomy and Astrophysics, 25:045007 (9pp), 2025 April

https://doi.org/10.1088/1674-4527/adbea3
CSTR: 32081.14.RAA.adbea3

Image Stabilization Residuals Caused by Tip-tilt of Fast Steering Mirror in the China Space Station Telescope

Long Li[1,2], Cheng-Hao Li[1], Quan Zhang[3], Yuan-Peng Gao[3], Zi-Huang Cao[2,4], Zhi-Rui Cao[1,2], Xu He[1,2], Li-Hao Zhang[1], and Wei Wang[1,2]

[1] Changchun Institute of Optics, Fine Mechanics and Physics, Chinese Academy of Sciences, Changchun 130033, China; wangwei123@ciomp.ac.cn
[2] University of Chinese Academy of Sciences, Beijing 100049, China
[3] Shanghai Institute of Technical Physics, Chinese Academy of Sciences, Shanghai 200083, China
[4] National Astronomical Observatories, Chinese Academy of Sciences, Beijing 100101, China
Received 2025 January 16; revised 2025 February 23; accepted 2025 March 7; published 2025 April 10

Abstract

The China Space Station Telescope (CSST) is a 2 m three-mirror anastigmat equipped with a Fast Steering Mirror (FSM), which is part of its precision image stabilization system. The FSM is used to compensate for residuals from the previous stage of the image stabilization system. However, a new type of image stabilization residual caused by image rotation and projection distortion is introduced when the FSM performs tip-tilt adjustments, reducing both the image stabilization accuracy and the absolute pointing accuracy of the CSST. In this paper, we propose a scheme to compute the image stabilization residuals across the full field of view (FOV) by using a reference star as the target for stabilization control, which can be utilized for subsequent image position correction. To achieve this, we developed a linear optical model for image point displacement by simplifying an existing image point displacement model and incorporating more readily available parameters. The computational accuracy of the new model is equivalent to that of the original, with computational differences of less than 0.03 μm. Based on this linear model, we established a calculation model for image stabilization residuals, including those due to image rotation and projection distortion caused by FSM tip-tilt adjustments. This model provides a theoretical foundation for quantifying such residuals during the image stabilization process. Finally, the results of testing using this scheme are provided. Experimental results demonstrate that within the observation FOV of the CSST, when the FSM tilts by ($1''$, $1''$), the maximum absolute value of the image stabilization residuals accounts for 20% of the total image stabilization accuracy requirement. This finding underscores the necessity of computing and correcting these residuals to meet performance requirements.

Key words: telescopes – techniques: image processing – methods: analytical

1. Introduction

The China Space Station Telescope (CSST) features a 2 m diameter aperture telescope, which adopts the Cook-type off-axis three-mirror anastigmat optical design and is equipped with five first-generation instruments: the Main Survey Camera, Integral Field Spectrograph, Multi-Channel Imager, Cool Planets Imaging Coronagraph, and High Sensitivity Terahertz Detection Module (Feng et al. 2024b; Zhan 2021). It is designed to enable large-area, high-resolution multi-color imaging and seamless spectroscopic surveys, as well as facilitate detailed studies of selected celestial objects and regions (Zhan 2021). One of the scientific requirements is that image stabilization accuracy must be better than $0\farcs05$, with a 3σ confidence level over 300 s, using a guide star (Feng et al. 2024a). To achieve this target, the CSST employs a precision image stabilization system that incorporates both the Fine Guidance Sensor (FGS) and the Fast Steering Mirror (FSM). During the image stabilization process, the FGS measures the centroid offset of the guide star and provides this data to the FSM control system. The control system then adjusts the FSM's position to correct for residual errors from the previous stage of the image stability system. However, because the FSM in the CSST is located within the convergent optical path and is not aligned with the exit pupil, the image motion (centroid error) at various angles of the Field of View (FOV) becomes unsynchronized during tip-tilt adjustments of the FSM. This discrepancy leads to inaccurate residual compensation for other field points when using the guide star on the FGS as a reference. It also results in new image stabilization residuals, including image rotation and projection distortion, thereby reducing image stabilization accuracy (Li et al. 2024). To further enhance image stabilization accuracy, these residuals need to be modeled, calculated, and corrected.

Notably, during the optical modeling activities for the James Webb Space Telescope (JWST) project, a linear optical model based on the linear system theory was introduced for a single

field point. This model simulated the FSM's tip and tilt while mapping structural displacements from static or dynamic loads into changes in the wave front at the exit pupil or centroids at the image surface through matrix representations of the optics, utilizing ray tracing to determine centroid and wave front error sensitivities (Howard 2004). Additionally, to predict the performance of each JWST instrument, the linear optical model was expanded to cover multiple field points. This revealed sensitivity variations between different field points relative to the central field point, with maximum discrepancies reaching nearly three parts in 1000 (excluding bulk observatory motion), highlighting the necessity of incorporating FSM motion effects to improve the model's accuracy in future work (Howard & Ha 2004). In the Large UV/Optical/Infrared Surveyor, the linear optical model and sensitivity matrix method were applied to examine how FSM disturbances impact overall optical system performance, aiming to identify all potential error sources early in the mission design (Sacks et al. 2019).

In our previous studies, a nonlinear model was constructed to describe the relationship between image point displacement and FSM tip-tilt angles based on geometrical optics theory. This model achieved a high computational accuracy of 0.01 μm, meeting the requirements for calculating image point displacement and numerically analyzing projection distortion effects. However, its complexity and the difficulty of obtaining its parameters in engineering applications limited its practical use (Li et al. 2024). In this paper, we first simplify the existing model and establish a linearized model. Based on this linear model, we develop a computational model for the image stabilization residuals, including image rotation and projection distortion, caused by the tip-tilt of FSM. Finally, we propose a solution that utilizes these models to compute the image stabilization residuals during the precise image stabilization process, and present the calculation results of this solution as applied in the CSST performance tests. This provides a theoretical foundation and data for subsequent image point position corrections.

2. Linearize the Model of Image Point Displacement Caused by Tip-tilt of FSM

In previous studies, we established a nonlinear model, as shown in formula (1), describing the relationship between image point displacement and the tip-tilt angles of the FSM, where the position of the observed target is represented by the direction vector of the chief ray incident on the surface of the FSM (Li et al. 2024). In this section, we simplify this model by introducing parameters that are easier to determine and using the FOV to represent the position of the observed target and linearize this model by taking the first-order approximation of the tip-tilt angles.

Table 1
Parameters in the Established Model and Their Meanings

Parameters	Their Meanings
(A_x, A_y, A_z)	Direction vector of the chief ray incident on the FSM
(N_{ox}, N_{oy}, N_{oz})	FSM's normal vector before its tip-tilt motion
(N_{tx}, N_{ty}, N_{tz})	FSM's normal vector after its tip-tilt motion
(x_0, y_0, z_0)	Coordinates of the FSM rotation center
(x_1, y_1, z_1)	Coordinates of the exit pupil center

$$\begin{cases}\Delta x = A_x(K_t - K_o) + A_z(K_oL_o - K_tL_t) + z_1(L_o - L_t)\\ \Delta y = A_y(K_t - K_o) + A_z(K_oM_o - K_tM_t) + z_1(M_o - M_t)\\ \Delta z = 0\end{cases} \tag{1}$$

in this model,

$$K_o = \frac{N_{ox}(x_0 - x_1) + N_{oy}(y_0 - y_1) + N_{oz}(z_0 - z_1)}{A_xN_{ox} + A_yN_{oy} + A_zN_{oz}},$$

$$K_t = \frac{N_{tx}(x_0 - x_1) + N_{ty}(y_0 - y_1) + N_{tz}(z_0 - z_1)}{A_xN_{tx} + A_yN_{ty} + A_zN_{tz}},$$

$$L_o = \frac{A_x(1 - 2N_{ox}^2) - 2A_yN_{ox}N_{oy} - 2A_zN_{ox}N_{oz}}{A_z(1 - 2N_{oz}^2) - 2A_xN_{ox}N_{oz} - 2A_yN_{oy}N_{oz}},$$

$$L_t = \frac{A_x(1 - 2N_{tx}^2) - 2A_yN_{tx}N_{ty} - 2A_zN_{tx}N_{tz}}{A_z(1 - 2N_{tz}^2) - 2A_xN_{tx}N_{tz} - 2A_yN_{ty}N_{tz}},$$

$$M_o = \frac{A_y(1 - 2N_{oy}^2) - 2A_xN_{ox}N_{oy} - 2A_zN_{oy}N_{oz}}{A_z(1 - 2N_{oz}^2) - 2A_xN_{ox}N_{oz} - 2A_yN_{oy}N_{oz}},$$

$$M_t = \frac{A_y(1 - 2N_{ty}^2) - 2A_xN_{tx}N_{ty} - 2A_zN_{ty}N_{tz}}{A_z(1 - 2N_{tz}^2) - 2A_xN_{tx}N_{tz} - 2A_yN_{ty}N_{tz}}.$$

The other parameters and their meanings are listed in Table 1. These parameters are expressed in the focal plane coordinate system, which is a right-handed system. In this coordinate system, the origin (o) is the image point of the center FOV, with the sagittal direction along the x-axis, the meridional direction along the y-axis, and the normal direction along the z-axis (Li et al. 2024).

To simplify formula (1), we approximate the trigonometric functions as $\sin\Delta\alpha \approx \Delta\alpha$, $\cos\Delta\alpha \approx 1$, $\sin\Delta\beta \approx \Delta\beta$, and $\cos\Delta\beta \approx 1$, thereby eliminating second-order and higher-order terms of the tip-tilt angles, as these angles are typically on the order of arcseconds in a precision image stabilization system. To make the model parameters more accessible for practical applications, we define the following: (X, Y) are FOV coordinates in object space, D is the vertical distance from the FSM's rotation center to the focal plane, F is the focal length, U is the angular magnification and (θ_x, θ_y) are the incidence angles of the chief ray at the central FOV on the focal plane. Thus, for an object at infinity

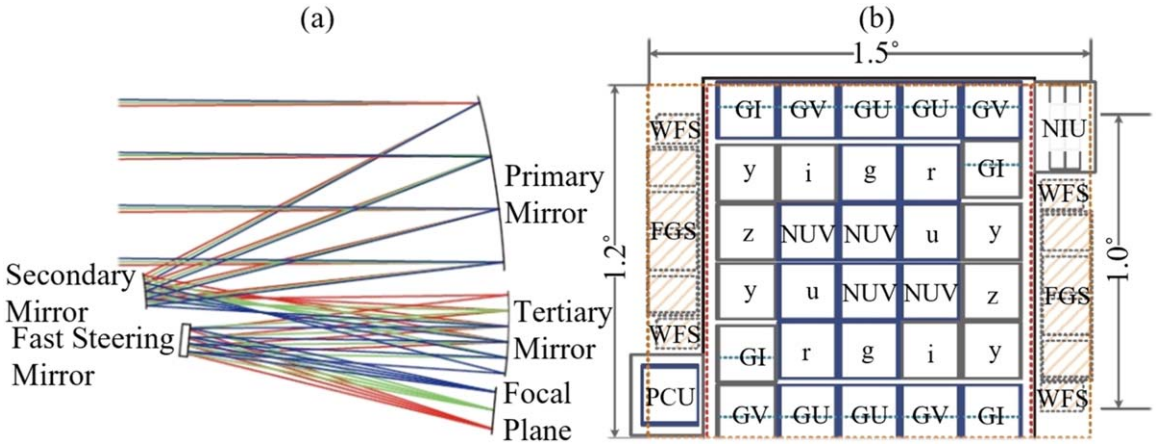

Figure 1. Illustration of (a) the optical design and (b) focal plane arrangement of the CSST survey camera (Zhan 2021).

with a field angle of (X, Y), the image point position and the direction vector of the chief ray incident on the focal plane are given by $(F\tan X, F\tan Y, 0)$ and$(\tan(\theta_x + UX), \tan(\theta_y + UY), 1)$, respectively (Kingslake & Johnson 2009). The equations in the model can be simplified to:

$$\begin{cases} A_x(-K_o) + A_z K_o L_o + z_1 L_o = x_1 - F\tan X \\ A_y(-K_o) + A_z K_o M_o + z_1 M_0 = y_1 - F\tan Y) \end{cases} \tag{2}$$

$$\begin{cases} L_o = \tan(\theta_x + UX) \\ M_0 = \tan(\theta_y + UY) \end{cases} \tag{3}$$

Finally, a linear optical model of image point displacement, represented in matrix form, is established using these simplified equations and redefined parameters. This model is:

$$\begin{bmatrix} \Delta x \\ \Delta y \end{bmatrix} = 2\begin{bmatrix} E_x \cdot A & E_y \cdot A \\ E_x \cdot B & E_y \cdot B \end{bmatrix}\begin{bmatrix} \Delta\alpha \\ \Delta\beta \end{bmatrix} \tag{4}$$

In this model, the image point displacement caused by the FSM's tip-tilt is expressed as $(\Delta x, \Delta y, 0)$, with the FSM's tip-tilt angles denoted as $(\Delta\alpha, \Delta\beta)$. The direction vectors of the FSM's sagittal and meridional rotation axes are represented as $\boldsymbol{E}_x = (a, b, c)^T$ and $\boldsymbol{E}_y = (d, e, f)^T$, respectively. Meanwhile,

$$A = \begin{bmatrix} (F\tan Y + D\tan\theta_y)\tan(\theta_x + UX) \\ -(F\tan X + D\tan\theta_x)\tan(\theta_x + UX) - D \\ F\tan Y + D\tan\theta_y \end{bmatrix} \tag{5}$$

$$B = \begin{bmatrix} (F\tan Y + D\tan\theta_y)\tan(\theta_y + UY) + D \\ -(F\tan X + D\tan\theta_x)\tan(\theta_y + UY) \\ -F\tan X - D\tan\theta_x \end{bmatrix} \tag{6}$$

To verify the computational accuracy of the simplified model, we will use the design parameters of the CSST to cross-validate the calculated results of both the old and new models. The design diagram of the CSST optical system and the focal plane arrangement of the CSST survey camera are shown in Figure 1 (Zhan 2021). We select the viewpoint $(-0.^\circ65, 0.^\circ40)$from the FOV range of the FGS in the focal plane of the CSST survey camera, and the tip-tilt angles of the FSM range from $-17.''5$ to $17.''5$ for cross-validation. The results show that the calculation accuracy of both models is comparable, with the maximum absolute differences in the x and y directions being 0.02 μm and 0.03 μm, respectively. When converted into angular distance in object space, these differences correspond to 1.5×10^{-4} arcsec and 2.2×10^{-4} arcsec, both of which are much smaller than the image stabilization accuracy requirements, it can meet the accuracy requirements of engineering applications.

3. Image Stabilization Residuals Caused by Tip-tilt of FSM

Figure 2 shows a schematic of the image positions on the CSST focal plane, consisting of nine image points within a $1.^\circ5 \times 1.^\circ2$ FOV, both before and after the FSM tip-tilt, with the displacement of each point magnified 3000 times to clearly highlight the changes in the image. It can be seen that the FSM's tip-tilt produces three effects: image translation, image rotation, and projection distortion. Among these, image translation is the most significant and forms the basic principle for the FSM to compensate for residuals from the previous stage of the image stability system. Image rotation and projection distortion, on the other hand, are additional effects and residuals (Li et al. 2024). In this section, we will develop calculation models for image translation and image stabilization residuals (including image rotation and projection distortion) by decoupling the linear optical model of image point displacement.

When the image point at the center of FOV is taken as a reference, the image point displacement (x_t, y_t)caused by image translation is equivalent to the image point displacement at the center of FOV. By substituting $X = 0^\circ$ and $Y = 0^\circ$ into

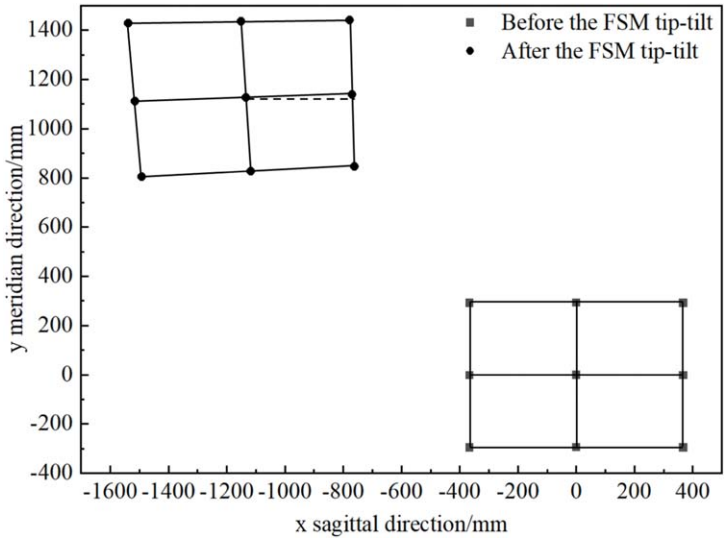

Figure 2. Images composed of nine FOV image points on the focal plane, both before and after the FSM tip-tilt.

Table 2
Summary of Established Linear Models

Effects Caused by FSM Tip-tilt	Sensitivity Matrix	Model's Difference
Image point displacement (Δx, Δy)	$2\begin{bmatrix} E_x \cdot A & E_y \cdot A \\ E_x \cdot B & E_y \cdot B \end{bmatrix}$	A, B
Image translation (x_t, y_t)	$2\begin{bmatrix} E_x \cdot A_t & E_y \cdot A_t \\ E_x \cdot B_t & E_y \cdot B_t \end{bmatrix}$	A_t, B_t
Image stabilization residuals (x_R, y_R)	$2\begin{bmatrix} E_x \cdot A_R & E_y \cdot A_R \\ E_x \cdot B_R & E_y \cdot B_R \end{bmatrix}$	A_R, B_R
Image rotation (x_r, y_r)	$2\begin{bmatrix} E_x \cdot A_r & E_y \cdot A_r \\ E_x \cdot B_r & E_y \cdot B_r \end{bmatrix}$	A_r, B_r
Projection distortion (x_d, y_d)	$2\begin{bmatrix} E_x \cdot A_d & E_y \cdot A_d \\ E_x \cdot B_d & E_y \cdot B_d \end{bmatrix}$	A_d, B_d

(Δx, Δy), it can be obtained as:

$$\begin{bmatrix} x_t \\ y_t \end{bmatrix} = 2\begin{bmatrix} E_x \cdot A_t & E_y \cdot A_t \\ E_x \cdot B_t & E_y \cdot B_t \end{bmatrix}\begin{bmatrix} \Delta\alpha \\ \Delta\beta \end{bmatrix} \tag{7}$$

where

$$A_t = D\begin{bmatrix} \tan\theta_x \tan\theta_y \\ -\tan^2\theta_x - 1 \\ \tan\theta_y \end{bmatrix} \tag{8}$$

$$B_t = D\begin{bmatrix} \tan^2\theta_y + 1 \\ -\tan\theta_x \tan\theta_y \\ -\tan\theta_x \end{bmatrix} \tag{9}$$

Therefore, the image stabilization residuals are equal to the difference in image point displacement between the other FOVs and the central FOV, namely:

$$\begin{bmatrix} x_R \\ y_R \end{bmatrix} = 2\begin{bmatrix} E_x \cdot A_R & E_y \cdot A_R \\ E_x \cdot B_R & E_y \cdot B_R \end{bmatrix}\begin{bmatrix} \Delta\alpha \\ \Delta\beta \end{bmatrix} \tag{10}$$

where

$$A_R = \begin{bmatrix} (F\tan Y + D\tan\theta_y)\tan(\theta_x + UX) - D\tan\theta_x\tan\theta_y \\ -(F\tan X + D\tan\theta_x)\tan(\theta_x + UX) + D\tan^2\theta_x \\ F\tan Y \end{bmatrix} \tag{11}$$

$$B_R = \begin{bmatrix} (F\tan Y + D\tan\theta_y)\tan(\theta_y + UY) - D\tan^2\theta_y \\ -(F\tan X + D\tan\theta_x)\tan(\theta_y + UY) + D\tan\theta_x\tan\theta_y \\ -F\tan X \end{bmatrix} \tag{12}$$

If the FOV corresponding to an image point on the focal plane is (X, Y), its position coordinate is ($F\tan X$, $F\tan Y$, 0). When the image undergoes a counterclockwise rotation by a small angle θ around the z-axis, the image point displacement (x_r, y_r) caused by the image rotation is $-\theta(F\tan Y, -F\tan X)$ by the approximation $\sin\theta \approx \theta$ and $\cos\theta \approx 1$. This can be expressed in the form of the linear sensitivity matrix as:

$$\begin{bmatrix} x_r \\ y_r \end{bmatrix} = 2\begin{bmatrix} E_x \cdot A_r & E_y \cdot A_r \\ E_x \cdot B_r & E_y \cdot B_r \end{bmatrix}\begin{bmatrix} \Delta\alpha \\ \Delta\beta \end{bmatrix} \tag{13}$$

where

$$A_r = \begin{bmatrix} 0 \\ 0 \\ F\tan Y \end{bmatrix} \tag{14}$$

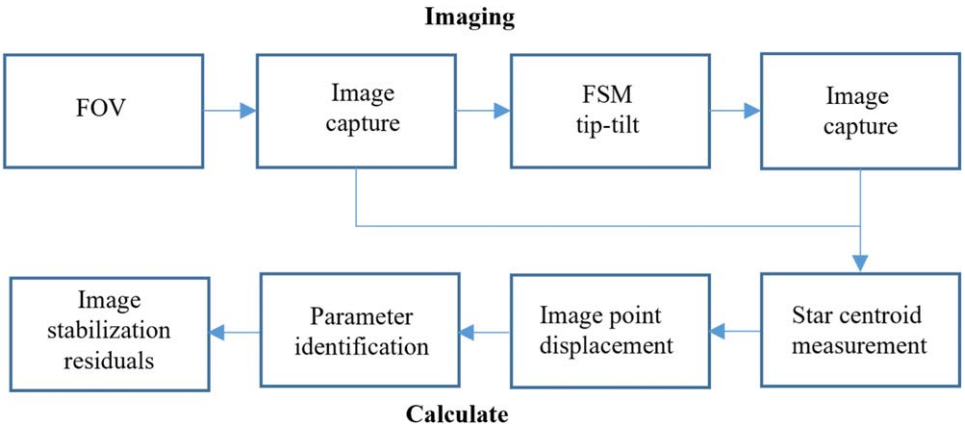

Figure 3. The main process to calculate image stabilization residuals caused by the FSM tip-tilt.

Table 3
Parameters in Sensitivity Matrix and Their Meaning

Parameters	Their Meaning
(X, Y)	Field of view
$E_x = (a, b, c)$	Direction vector of the FSM's sagittal axis
$E_y = (d, e, f)$	Direction vector of the FSM's meridian axis
D	Vertical distance from the FSM's rotation center to the focal plane
F	Focal length
U	Angular magnification
(θ_x, θ_y)	Incidence angles of the chief ray at the central FOV on the focal plane

$$B_r = \begin{bmatrix} 0 \\ 0 \\ -F\tan X \end{bmatrix} \tag{15}$$

and the angle of image rotation is

$$\theta = -2(c\Delta\alpha + f\Delta\beta) \tag{16}$$

Thus, the image point displacement (x_d, y_d) caused by projection distortion is equal to the difference between (x_R, y_R) and (x_r, y_r), namely:

$$\begin{bmatrix} x_d \\ y_d \end{bmatrix} = 2\begin{bmatrix} E_x \cdot A_d & E_y \cdot A_d \\ E_x \cdot B_d & E_y \cdot B_d \end{bmatrix}\begin{bmatrix} \Delta\alpha \\ \Delta\beta \end{bmatrix} \tag{17}$$

where

$$A_d = \begin{bmatrix} (F\tan Y + D\tan\theta_y)\tan(\theta_x + UX) - D\tan\theta_x\tan\theta_y \\ -(F\tan X + D\tan\theta_x)\tan(\theta_x + UX) + D\tan^2\theta_x \\ 0 \end{bmatrix} \tag{18}$$

$$B_d = \begin{bmatrix} (F\tan Y + D\tan\theta_y)\tan(\theta_y + UY) - D\tan^2\theta_y \\ -(F\tan X + D\tan\theta_x)\tan(\theta_y + UY) + D\tan\theta_x\tan\theta_y \\ 0 \end{bmatrix} \tag{19}$$

Tables 2 and 3 present the linear models established in this section, along with all the parameters and their respective meanings. As shown in the tables, these models share the same structure, with the only difference being the proportional coefficient matrix related to the tip-tilt angles $(\Delta\alpha, \Delta\beta)$, also known as the sensitivity matrix. From the linear model of the image stabilization residuals, it is evident that when the FOV remains constant, the sensitivity matrix also remains unchanged. The image stabilization residuals (including image rotation and projection distortion) are proportional to the tip-tilt angles of the FSM, and the proportional coefficients can be easily determined using commonly used methods, such as the least squares algorithm. However, when the FOV changes, the proportional coefficients exhibit a nonlinear relationship with the FOV, which makes pre-calibration and correction more difficult. Therefore, it is essential to develop a method that computes these residuals in real time during the image stabilization process, enabling real-time correction.

4. Calculating Image Stabilization Residuals During Precision Image Stabilization Process

The premise for correcting image stabilization residuals caused by the FSM's tip-tilt during the precision image stabilization process is knowing the values of these residuals for a single FOV or even the full FOV after the FSM has been tilted at any angle. This section proposes a feasible scheme for obtaining these data using the established models in engineering applications, which was also used in relevant CSST tests. The scheme is shown in Figure 3 and consists of two main steps: imaging and calculation. In the first step, the FGS captures an image of a star in a specific

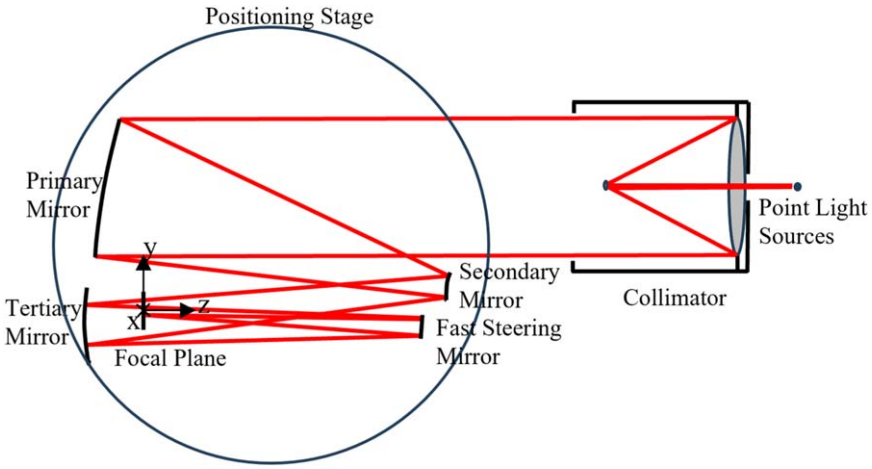

Figure 4. The experimental equipment and optical path.

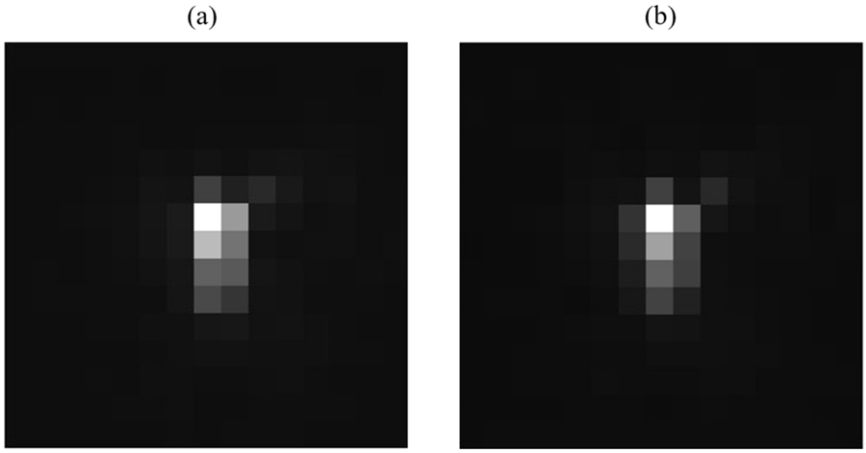

Figure 5. Window image of the FOV at (−0.°65, 0.°40) when the FSM tip-tilts by (a) (0″, 0″) and (b) (−3″, 0″).

FOV before and after the FSM's tip-tilt. In the second step, the process involves: using a subpixel centroid extraction algorithm to measure the centroids of the images, calculating the image point displacements by subtracting the centroid coordinates of the two images taken before and after the FSM tip-tilt, applying an optimization algorithm to identify parameters in the image point displacement model based on these data as the parameters may differ from these design values due to factors such as manufacturing and assembly and incorporating the identified parameters into the image stabilization residuals model to calculate the image stabilization residuals (including image rotation and projection distortion) for the full FOV after the FSM tip-tilt.

To verify the feasibility of the above scheme when the CSST is in orbit, the experimental optical setup shown in Figure 4 was used. Point light sources and a collimator were employed to simulate a guide star at infinity, with its position changing within the CSST's FOV by tip-tilting the positioning stage. The on-orbit environment was simulated by placing the CSST on a gravity unloading device and conducting the entire experiment within a vacuum tank. Additionally, during the experiment, the definitions of the FOV and focal plane coordinate systems were as follows: The X direction of the FOV and the y direction of the focal plane represent the yaw direction, while the Y direction of the FOV and the x direction of the focal plane represent the pitch direction.

First, the simulated guide star was placed at (−0.°65, 0.°40) within the FOV range of the FGS. The tip-tilt angles of the FSM were varied 24 times within its working angles to capture images, measure centroids using the grayscale centroid method, and calculate image point displacements. The results are shown in Figure 5 and Table 4.

These tip-tilt angles and corresponding image point displacements were input into the linear model of image point displacement, and the model parameters were identified. For the parameter identification of linear models, Ordinary Least Squares (OLS) was applied to obtain the proportionality

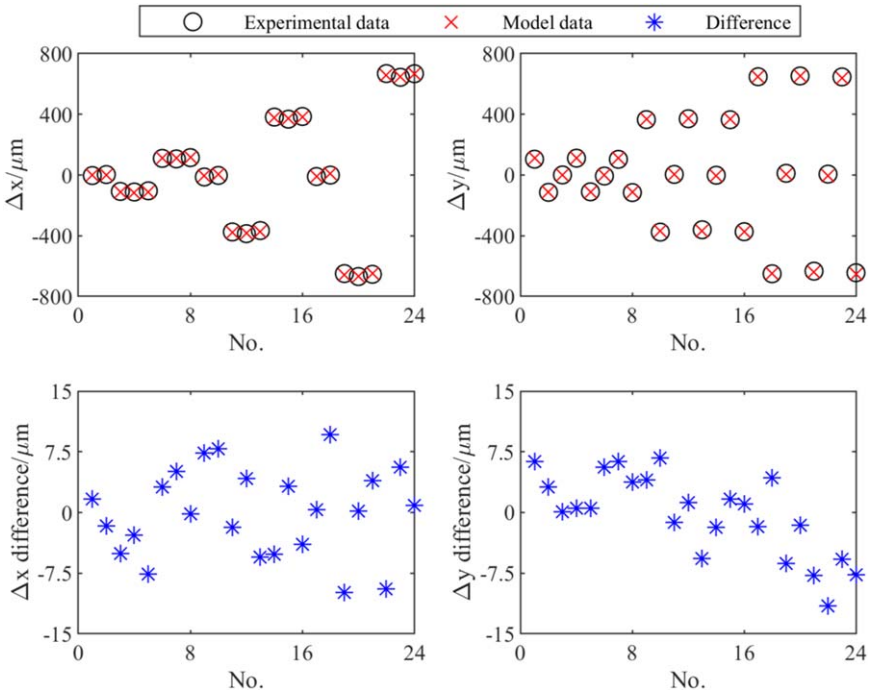

Figure 6. Image point displacement and difference between model data through OLS and experimental data.

Table 4
Spectral Parameters and Black Hole Masses of Six New Quasars

No.	$\Delta\alpha/''$	$\Delta\beta/''$	Δx/mm	Δy/mm	No.	$\Delta\alpha/''$	$\Delta\beta/''$	Δx/mm	Δy/mm	No.	$\Delta\alpha/''$	$\Delta\beta/''$	Δx/mm	Δy/mm
1	−3	0	−3.23	110.48	9	−10	0	−12.71	371.23	17	−17.5	0	−9.73	653.95
2	3	0	3.32	−107.93	10	10	0	−2.55	−370.03	18	17.5	0	−0.28	−644.55
3	0	−3	−107.94	6.83	11	0	−10	−374.88	10.21	19	0	−17.5	−649.39	17.54
4	−3	−3	−111.80	117.15	12	−10	−10	−386.26	377.05	20	−17.5	−17.5	−668.83	659.02
5	3	−3	−103.81	−104.43	13	10	−10	−365.88	−354.60	21	17.5	−17.5	−653.90	−627.26
6	0	3	109.86	−0.48	14	0	10	381.97	4.82	22	0	17.5	668.75	12.29
7	−3	3	106.36	109.55	15	−10	10	368.21	370.60	23	−17.5	17.5	644.38	652.75
8	3	3	114.86	−109.41	16	10	10	386.06	−367.32	24	17.5	17.5	667.85	−637.75

coefficients ($2E_x \cdot A$, $2E_y \cdot A$, $2E_x \cdot B$, and $2E_y \cdot B$) between (Δx, Δy) and ($\Delta\alpha$, $\Delta\beta$), as shown in Table 2 and Figure 6. This also allowed for the determination of system errors that could be corrected in the experiment.

From the data in Table 5, it can be observed that due to the use of a gravity unloading device to counterbalance the CSST's weight, when the pointing platform shifts as the position of the simulated star in the FOV is changed, the gravity unloading device adjusts to maintain force equilibrium. This causes the CSST to move slowly, introducing system errors of 0.017 μm and 5.989 μm in the experimental data. Meanwhile, the Δy, corresponding to the yaw direction, results in a larger offset when adjusting the guide star's FOV position, thereby leading to greater displacement on the focal plane. Additionally, random errors are introduced by factors such as changes in the energy and shape of the image spot caused by environmental vibrations, as shown in Figure 6. These variations, which affect the centroid position, result in the Root Mean Square Error (RMSE) between the model calculation data and the experimental data being 5.205 μm in Δx and 4.979 μm in Δy, respectively.

Subsequently, to resolve the residuals during the image stabilization process, we employed a Gradient Descent (GD) algorithm to derive consistent parameters for both the image point displacement model and the image stabilization residuals model, after removing the identified systematic errors. In this study, the GD was applied with the RMSE—calculated as the root mean square of the RMSE values for Δx and Δy—as the objective function, and the design values of these parameters were used as initial values in the optimization process. The goal was to optimize the pose parameters of the FSM and the optical

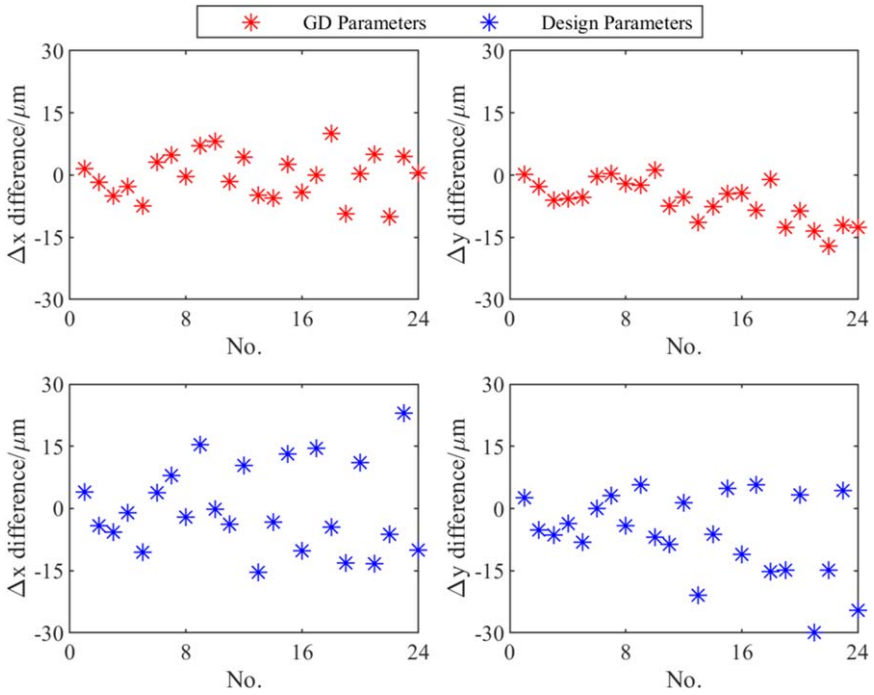

Figure 7. Difference of image point displacement between model data using the parameters obtained from the GD, their design values, and test data.

Table 5
The Model Parameters and Errors are Obtained by OLS

$2E_x \cdot A/$ (μm/″)	$2E_y \cdot A/$ (μm/″)	C_x/μm	RMSE(Δx)/μm
−0.558	−37.638	0.017	5.205
$2E_x \cdot B/$ (μm/″)	$2E_y \cdot B/$ (μm/″)	C_y/μm	RMSE(Δy)/μm
36.886	0.277	5.989	4.979

Table 6
The Model Parameters and Errors are Obtained by GD

$2E_x \cdot A/$ (μm/″)	$2E_y \cdot A/$ (μm/″)	$2E_x \cdot B/$ (μm/″)	$2E_y \cdot B/$ (μm/″)	RMSE/μm
−0.558	−37.638	36.886	0.277	5.092

system parameters, including (a, b, c), (d, e, f), D, F, U, θ_x, and θ_y. To cross-validate the results obtained by the GD with the OLS, the parameters obtained by the GD are converted into proportionality coefficients between $(\Delta x, \Delta y)$ and $(\Delta\alpha, \Delta\beta)$, as shown in Table 6.

From the data in Tables 5 and 6, it can be seen that these coefficients and RMSE values are identical, indicating that the parameter fitting results obtained through the GD have reached optimality and can be used to calculate the image stabilization residuals.

Meanwhile, as shown in Figure 7, the image point displacements calculated using the parameters obtained from the GD and their design values, when compared with the experimental raw data (Table 1), show that the results using the GD have smaller errors. The RMSE between the model calculation data and the experimental data are 6.624 μm and 10.681 μm, respectively. This indicates that after fitting the model parameters using the GD, the RMSE between the model calculation data and the experimental data was reduced by 38%. This also proves that the approach of performing model parameter identification before solving the image stabilization residuals can reduce the model's calculation error.

Finally, to provide data for full field-of-view stabilization residual correction, the parameters obtained through the GD algorithm, along with the stabilization residual model, can be used to calculate the stabilization residual values (including image rotation and projection distortion) for the entire FOV at any given tip-tilt angle. Figure 8 shows the calculated results for these residuals caused by the FSM tip-tilt at a tip-tilt angle of (1″, 1″), with the FOV range being $1.^{\circ}5 \times 1.^{\circ}2$. As shown in Figure 8(a), the minimum residual occurs at $(0.^{\circ}75, -0.^{\circ}60)$, with a value of approximately -1.285 μm. This corresponds to an angular distance of $0.''01$ in object space, which accounts for 20% of the total image stabilization accuracy requirement. This demonstrates that, during the precise image stabilization process, the residuals caused by FSM tip-tilt cannot be ignored when operating within a small stroke range. When the FSM operates at a large stroke range, the residuals exceed the

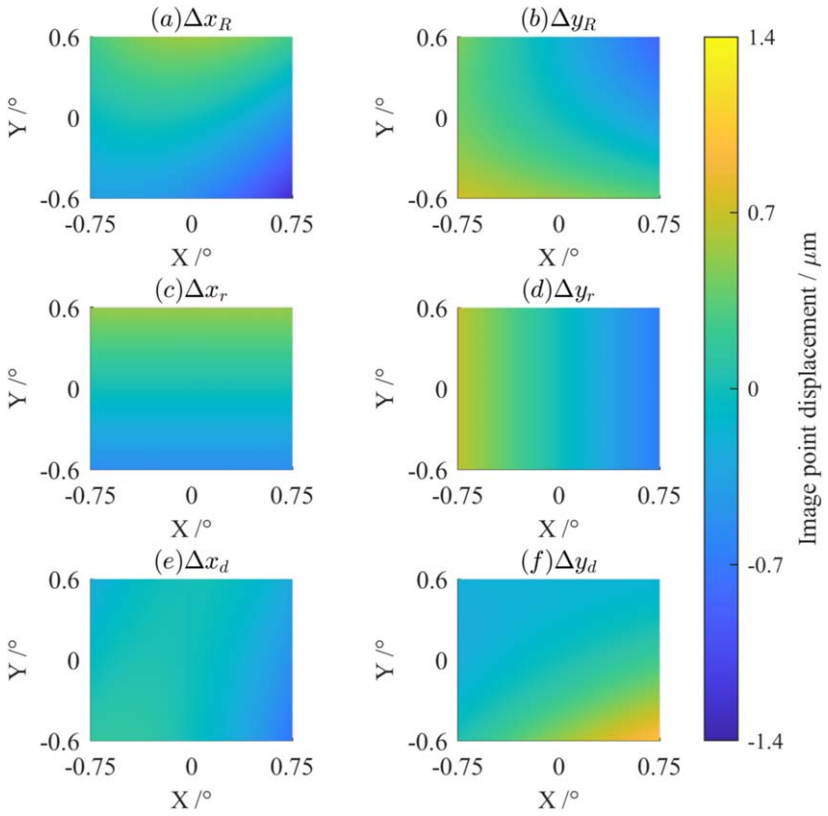

Figure 8. Image stabilization residuals for the full FOV at a tip-tilt angle of (1″, 1″).

stabilization accuracy requirements, highlighting the need for calculation and correction of these residuals.

5. Conclusion

To analyze and calculate the image stabilization residuals caused by the tip-tilt of the FSM in the CSST, we simplified the existing image displacement model and used more readily available parameters to establish a linear optical model of image point displacement. The computational accuracy of the new model is comparable to that of the original model, with computational differences of less than 0.03 μm. Based on this linear model, we developed a relationship between the image translation required for image stabilization and the FSM tilt angles, as well as a calculation model for the image stabilization residuals (including image rotation and projection distortion) caused by the FSM's tip-tilt. This model provides a theoretical basis for the angle control of the FSM and the calculation of image stabilization residuals during the image stabilization process. Using these models, we proposed a scheme to calculate the residuals, which was applied in relevant CSST tests. The experimental results show that, before solving the image stabilization residuals using the established model, applying the GD algorithm to identify the model parameters results in smaller errors compared to directly using the design values of the parameters. Additionally, within the CSST's observation FOV, the residuals caused by FSM tip-tilt cannot be ignored during the precise image stabilization process when operating within a small stroke range. When the FSM operates at a large stroke range, the residuals exceed the stabilization accuracy requirements, highlighting the need for their calculation and correction.

Acknowledgments

We thank the referees for their constructive report and the CSST image stabilization team for providing valuable technical support and experimental data. This work was financially supported by the National Key R&D Program of China (2022YFB3806300).

References

Feng, H.-M., Cao, Z.-H., Lam, M. I., et al. 2024a, RAA, 24, 045004
Feng, H.-M., Cao, Z.-H., Lam, M. I., et al. 2024b, RAA, 24, 095010
Howard, J. M. 2004, Proc. SPIE, 5178, 82
Howard, J. M., & Ha, K. 2004, Proc. SPIE, 5487, 850
Kingslake, R., & Johnson, R. B. 2009, Lens Design Fundamentals (2nd ed.; New York: Academic)
Li, L., Wang, W., Cao, Z.-R., Meng, Q.-Y., & Li, C.-H. 2024, AcOpS, 44, 66
Sacks, L. W., Collins, C., Walsh, G., et al. 2019, Proc. SPIE, 11115, 315
Zhan, H. 2021, ChSBu, 66, 1290